AIP | Review of Scientific Instruments

Vertical dispersion mode doublecrystal spectrometer for advanced spectroscopy of laserproduced plasma

O. Renner, M. Kopecký, J. S. Wark, H. He, and E. Förster

Citation: Review of Scientific Instruments **66**, 3234 (1995); doi: 10.1063/1.1145488
View online: http://dx.doi.org/10.1063/1.1145488
View Table of Contents: http://scitation.aip.org/content/aip/journal/rsi/66/5?ver=pdfcov
Published by the AIP Publishing

Vertical dispersion mode double-crystal spectrometer for advanced spectroscopy of laser-produced plasma

O. Renner and M. Kopecký
Institute of Physics, Academy of Sciences of the Czech Republic, 18040 Prague, Czech Republic

J. S. Wark and H. He
Department of Physics, Clarendon Laboratory, University of Oxford, Parks Road, Oxford, OX1 3PU, United Kingdom

E. Förster
X-ray Optics Group of Max-Planck-Gesellschaft at University of Jena, 07743 Jena, Germany

(Received 13 July 1994; accepted for publication 16 January 1995)

A vertical dispersion variant of the double-crystal spectrometer (DCV), which has been successfully used to study radiative transport in plasmas with large velocity gradients, is described. The full theory of the instrument is presented with particular reference to distortion of the spectral lines observed. The main characteristics of the DCV were computed by ray tracing procedures and compared with experiment. Due to its extremely high dispersion, the DCV minimizes geometric apparatus smearing, the distortion of the spectra is negligible a high spectral resolution (typically several thousand or better) can be achieved at relatively small source-to-detector distances. The instrument provides two sets of spectra with one-dimensional spatial resolution at the level of 10 μm, and its sensitivity to relative positions and shifts of the spectral lines may be estimated as one part in 10^5. The very high precision in wavelength determination, both absolute and relative, combined with an acceptable luminosity make this spectrometer especially useful for ultrahigh-resolution spectroscopy of laser-produced plasmas. © *1995 American Institute of Physics.*

I. INTRODUCTION

X-ray spectroscopy is a widely used diagnostic tool in the study of laser-produced plasmas (LPPs).[1] Plasma temperatures can be derived from the intensity ratio of lines emitted from ions of different charge states or, as has been shown more recently, by isoelectronic methods.[2] Densities can be inferred from the Stark-broadened profiles of optically thin resonance lines (if the spectral resolution of the instrument is sufficient) and from the intensities of lines having decay rates comparable to electron collision rates.

A number of spectroscopic schemes have been advocated for use in the diagnosis of LPPs: these include flat single-crystal spectrometers, von Hamos and toroidal focusing schemes,[3] instruments working in the Johann mode,[4] elliptically bent crystals,[5] and schemes involving the Renninger effect,[6] to mention the main ones. Each of these types of instruments has its own set of characteristics, advantages, and disadvantages, and care should be taken in choosing the correct instrument for a particular application.[7,8]

In this paper we present both calculations and experimental data on the performance of a relatively novel x-ray instrument: the vertical dispersion variant of the double-crystal x-ray spectrometer (DCV). The principle of this instrument was described by Hrdý[9] and its use for plasma spectroscopy was first suggested 10 years ago,[10] but it was not until very recently that it was fielded in a laser-plasma experiment.[11,12] This instrument has remarkable characteristics including a spectral resolution that can, in principle, exceed the single-crystal rocking curve limit, as well as yielding one-dimensional spatial resolution of a few micrometers. Furthermore, as will be described below, the instrument allows very accurate measurements of line shifts to be made due to its extremely high dispersion and production of two symmetric spectra around a single reference point. These features have allowed the effect of velocity gradients on line shapes and positions to be measured in the keV regime,[12] and, we believe, give the instrument distinct advantages over other spectroscopic schemes for certain types of experiments.

Although some of the characteristics of the instrument have been presented elsewhere,[11,13] a complete theoretical analysis of the luminosity, spectral, and spatial resolution of the instrument, and the merits of its performance relative to other spectroscopic schemes, is still outstanding. We present such an analysis here, and along side the calculations include experimental results demonstrating that the instrument performs in a manner consistent with the calculations. We first describe the instrument in detail, then outline the calculations performed, and finally compare the results of these calculations with the results of experiments.

II. PRINCIPLE OF DCV

The double-crystal spectrometer (DCS) with equispacing crystals in nonparallel $(n, +n)$ setting is a classic instrument for precise measurements of x-ray wavelengths or crystal lattice spacings.[14] A spectral window of the radiation transmitted through the spectrometer is given by the single-crystal diffraction pattern (SCDP) and the mutual angular position of the crystals used and represents typically a fraction of the spectral linewidth. The conventional DCS is based on dispersion in the plane of incidence defined by the x-ray source and the relevant reciprocal-lattice vectors of the crystals (hori-

 0034-6748/95/66(5)/3234/10/$6.00

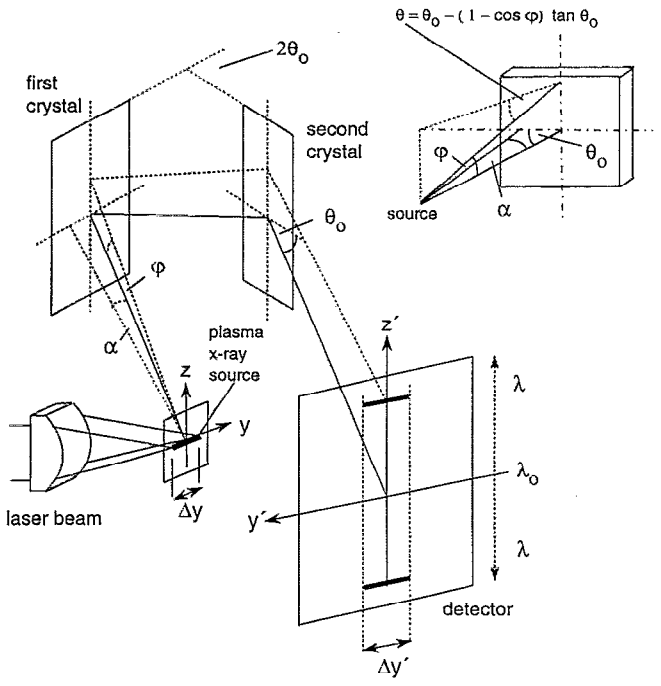

FIG. 1. Schematic diagram of the double-crystal spectrometer.

zontal plane). The profile of the investigated spectral lines is measured step by step by rotating one or both crystals, while the vertical divergence of the beam is considered as a distortion effect which is usually suppressed by a system of horizontal slits.

For obvious reasons (limited reproducibility and sometimes also very low frequency of x-ray pulses), this standard method cannot be applied to laser-plasma spectroscopy. One way to accommodate the pulsed character of these x-ray sources and to take spectroscopic data with a quality comparable to that of the conventional DCS is to use the vertical dispersion variant of the double-crystal spectrometer.

The main characteristics of the DCV can be understood from a schematic diagram of the experiment shown in Fig. 1. X rays emitted from LPP pass through a thin plastic foil which prevents heating of the first crystal and protects it against debris. The angle between the two crystals is set to be $2\theta_0$ so that the central beam which lies in the horizontal plane strikes both crystals at the Bragg angle θ_0 corresponding to the wavelength λ_0 (throughout the paper we suppose that diffraction planes are parallel to the crystal surface). As follows from the theory of DCS in $(n, +n)$ setting,[14] only the rays with negligible small horizontal divergence α are transmitted through the instrument. In contrast to the conventional DCS, the vertical divergence of the beam is not limited by slits and may even exceed 10°. The rays diffracted successively from both crystals are dispersed in the vertical direction and recorded at the detector (typically x-ray film or a CCD camera).

To understand the principle of dispersion in the vertical direction, consider the diffraction of an x-ray beam with negligible horizontal divergence from the single flat crystal. Now denote the horizontal glancing angle of a ray incident on the crystal by θ_0 and its vertical divergence angle by φ. From simple geometric consideration, the Bragg angle θ at which the ray strikes the crystal is given by

$$\sin\theta = \sin\theta_0 \cos\varphi, \tag{1}$$

which can be rewritten in the form

$$\theta = \theta_0 - (1 - \cos\varphi)\tan\theta_0. \tag{2}$$

According to Bragg's law, only that wavelength λ which satisfies the equation

$$\lambda = \lambda_0 \cos\varphi \tag{3}$$

is reflected at given φ. For each λ, reflection occurs at two angles $\pm\varphi$—the rays with the wavelengths shorter than λ_0 are dispersed in the vertical direction symmetrically about the horizontal plane containing the central beam.

Relation (3) holds universally and does not depend on the type of the crystal used; the only restriction is that the central ray satisfies the Bragg condition for the wavelength λ_0. The wavelength range covered is given by the span of φ and may be easily shifted by altering θ_0.

By differentiating Eq. (3) the vertical dispersion is

$$d\varphi/d\lambda = -1/(\lambda \tan\varphi), \tag{4}$$

while the dispersion in the horizontal plane follows from the Bragg condition, i.e.,

$$d\theta/d\lambda = \tan\theta/\lambda. \tag{5}$$

Both dispersions are identical for the Bragg angles $\theta = \pi/2 - \varphi$, i.e., at quasi-normal incidence of x rays. In other cases, the vertical dispersion is a factor $-1/(\tan\theta\tan\varphi)$ higher than that of the classical schemes with dispersion in the horizontal direction. High dispersion is an important parameter: it reduces the geometric apparatus smearing due to the finite size of the source so that the spectral resolution close to the diffraction limit of the given crystal can be achieved at a reasonable source-to-detector distance. Using extremely high dispersion at low angles φ, spectral line shifts and shapes may be accurately investigated; this is particularly true when the high dispersion is combined with another characteristic feature—the production of two sets of symmetrical spectra.

Equations (1)—(5) were derived for the diffraction from the flat single crystal; however, since the source has a finite horizontal dimension, the use of the single-crystal spectrometer in the vertical dispersion mode does not normally lead to a substantial increase in spectral resolution. This has already been discussed in a previous paper,[11] where alternative possibilities for achieving highly resolved spectra from LPP were also outlined.

In the case of the DCV this problem is overcome by a negligible horizontal divergence of the diffracted beam. To understand this, detailed theory of the instrument will be presented in the next section.

III. SURVEY OF DCV THEORY

The theory of the DCV is based on the integral equations of Compton and Allison[14] who derived an expression for the total power transmitted by the system of two crystals in an-

tiparallel configuration. Their approach is adequate to describe the properties of the conventional DCS under the assumption of small φ but it fails in the case of DCV, where the properties of the instrument are determined not by the integral diffracted intensity but by its spatial distribution at relatively high angles φ.

An analysis of the DCV starts from a modification of Eq. (4) of Renner and Kopecky.[13] In the system considered above where two perfect crystals in the $(n, +n)$ configuration are set symmetrically in relation to the central ray incident on both crystals at the Bragg angle θ_0, the irradiance P at the detector plane (y', z') is described by

$$P(y',z') = \int_\lambda \int_y \int_z T(\alpha,\varphi,\lambda) H(\alpha) G(\varphi) S(y,z) \times J(\lambda-\lambda_0) C(\alpha,\varphi,\lambda) F(\varphi,\lambda) d\lambda\, dy\, dz, \tag{6}$$

where $\alpha = \tan^{-1}[(y' - y)/L]$ and $\varphi = \tan^{-1}[(z' - z)/L]$; L is the source-to-detector distance via the crystals and the coordinate axes perpendicular to the central beam are defined in Fig. 1. T is the transmission efficiency through protective foils, H and G the source intensity profiles in the horizontal and vertical directions, S the distribution of the flux radiated by the source, and J the source spectral profile; for simplicity we assume that H, G, S, and J are mutually independent. The last two variables, a composite rocking curve C, and an intensity reduction factor F are decisive for the function of the DCV and we will discuss them in more detail.

The composite rocking curve (CRC) is defined by

$$C(\alpha,\varphi,\lambda) = C_{\mathrm{I}}[\alpha - (1-\cos\varphi)\tan\theta_0 - (\lambda-\lambda_0)D_0] \times C_{\mathrm{II}}[-\alpha - (1-\cos\varphi)\tan\theta_0 - (\lambda-\lambda_0)D_0], \tag{7}$$

where C_{I}, C_{II} are the single-crystal diffraction patterns of the crystals and $D_0 = \tan\theta_0/\lambda_0$ is the angular dispersion in the horizontal direction. The CRC determines the properties of the DCV: in contrast to the SCDP (which is defined as the ratio of diffracted and incident power dependent on the change of glancing angle in the plane of incidence), it provides a spatially limited two-dimensional distribution of monochromatic radiation diffracted at a given angular setting of the crystals. From the definition, the CRC is always symmetrical in the horizontal direction and its peak value is a constant given by multiplying the peak values of the two SCDPs, C_{I} and C_{II}. As these reach appreciable values only for $|\pm\alpha - (1 - \cos\varphi)\tan\theta_0 - (\lambda - \lambda_0)D_0| < \omega$, where ω is the full width of the SCDP at half maximum (in the wavelength range considered here, typically less than a few units or tens of arcseconds), a significant reflected power is observed only for rays with horizontal divergence close to zero. Simultaneously, a condition $(1-\cos\varphi)\tan\theta_0 = -(\lambda-\lambda_0)D_0$ must be fulfilled, i.e., at given angle φ we observe a quasi-monochromatic beam with the wavelength corresponding to Eq. (3). The FWHM value of the CRC in the horizontal direction Δw_h is slightly less than ω (it is a product of two SCDPs) and constant for all φ. In contrast, its width Δw_v in the vertical direction strongly depends on φ and is a factor of $1/(\tan\theta\tan\varphi)$ higher than Δw_h.

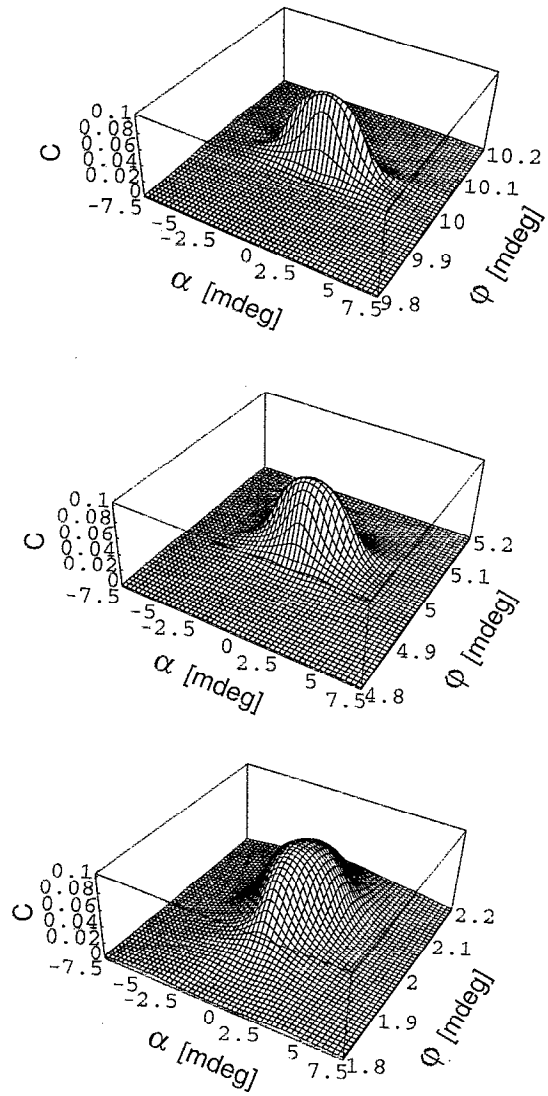

FIG. 2. Composite rocking curve C of the DCV. Its width in the direction of horizontal divergence α is constant but in the other direction it strongly depends on the vertical divergence angle φ.

This is illustrated in Fig. 2. The function $C(\alpha,\varphi,\lambda)$ has been computed for monochromatic radiation with the wavelength 7.1749 Å corresponding to the spectral line Al $Ly\alpha_{1/2}$. This radiation was diffracted from crystals of ADP (ammonium dihydrogen phosphate) (101) with the refractive index-corrected value of $2d = 10.638$ Å. The structure factors necessary to calculate the SCDP were taken from a program package DIXI3.[15] The computed width of the SCDP for an unpolarized beam is $\omega = 6.4$ mdeg, whereas the horizontal width $\Delta w_h = 4.9$ mdeg. The CRC may be understood as an angular distribution of transmitted power corresponding to a point source, i.e., a point spread function.

Thus the DCV provides spectra with 1D spatial resolution perpendicular to the dispersion direction. As may be seen from Figs. 1 and 2, individual sections of the source give an origin to the system of vertical dispersion planes; the

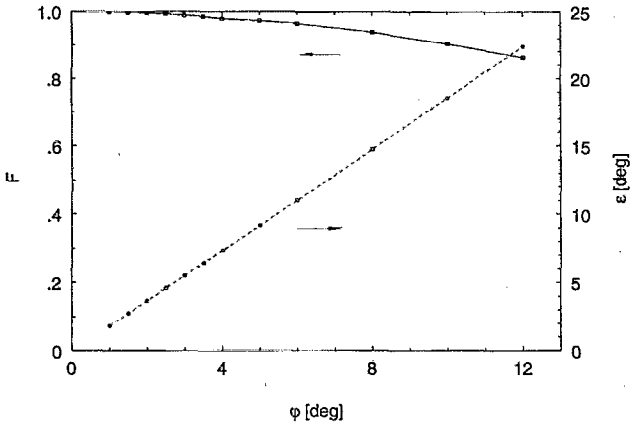

FIG. 3. The power transmitted through the DCV is reduced by the factor F depending on the angle of partial crossing of polarization vectors ϵ.

source is projected onto the detector at unit magnification. Assuming the source is a line extended in the direction of the y axis and is monochromatic, then its image will again be the line parallel to y' and broadened by the finite values of Δw_h and Δw_v. In practice, the vertical width of the image will be much higher due to the dispersion of the spectral line profile.

The spatial resolution is limited by $\Delta w_h L$ and for $L=100$ mm it corresponds to 8.5 μm. The obvious way to improve the spatial resolution is to use crystals with a narrower SCDP and/or to shorten the source-to-detector distance L. Either of these possibilities will slightly deteriorate some properties of the instrument. In the first case the luminosity and in the second case the spectral resolution of the DCV will decrease. There is always some trade-off among the luminosity and the spectral and spatial resolution.

The factor F in Eq. (6) takes into account a reduction of the transmitted power due to the partial crossing of polarization vectors of radiation diffracted from the first and the second crystal.[16] For unpolarized emission this may be expressed as

$$F(\varphi,\lambda)=\cos\varphi(\cos^2\epsilon+2\sin^2\epsilon|\cos 2\theta| + \cos^2\epsilon\cos^2 2\theta)/(1+\cos^2 2\theta), \quad (8)$$

where the angle ϵ between the crossed electric-field vectors of a given polarization component (σ or π) follows from

$$\cos\epsilon=1-2\sin^2\theta_0\tan^2\varphi/(\cos^2\theta_0+\tan^2\varphi). \quad (9)$$

The values of F and ϵ calculated for the same parameters as above are shown in Fig. 3. The angle ϵ depends almost linearly on φ in the given range. Even under relatively unfavorable conditions (at the Bragg angle close to 45°, where the π-polarization component is strongly suppressed) the intensity reduction may be neglected up to approximately $\varphi=8°$ (which corresponds to $F=0.94$). At higher angles φ, this decrease must be taken into account.

Many relevant parameters of the DCV (spectral range, dispersion, and spatial resolution) can be computed from the theory given above. However, at least two important characteristics, the luminosity and spectral resolution of the instrument, cannot be discussed on the basis of simple analytic formulas. These parameters were determined by using a ray tracing code, from which the main results are presented in Sec. IV.

IV. EVALUATION OF THE DCV CHARACTERISTICS

To perform a quantitative analysis of the DCV, the integration in Eq. (6) has been replaced by a summation. The details of the ray tracing procedure are described elsewhere;[13] only those parameters which are substantial for understanding the computed results are explained here.

All the data were calculated for a two-dimensional homogeneous and isotropic source perpendicular to the central beam. The spectral profile was represented either by a δ function or by Lorentzian or Gaussian spectral profiles with different FWHM values $\Delta\lambda$. The calculations were extended to asymmetric spectral lines, by introducing an asymmetry factor $a=\Delta\lambda_1/\Delta\lambda_s$ into the profiles; here $\Delta\lambda=\Delta\lambda_1+\Delta\lambda_s$ and $\Delta\lambda_1$ and $\Delta\lambda_s$ are, respectively, the wavelength differences from the peak on the long- and short-wavelength sides. A unit radiation power emitted from 1 mm^2 of the source into a solid angle 1 mrad^2 was assumed both in the case of monochromatic radiation and in the integrated profiles of the spectral lines. The intensity distribution at the detector plane was calculated from the ray tracing procedure by assuming that the radiation is reflected from the crystal surface in accordance with the dynamical theory of diffraction. The spectral resolving power $R=\lambda/\Delta\lambda$ was then determined from the FWHM value $\Delta\lambda$ given by the monochromatic signal distribution. The luminosity B was defined as the value proportional to the maximum signal at the detector. For convenience, in the graphs B is represented in units of mrad^2; the actual signal at the detector may be obtained by multiplying B by the source radiance in units of x/(mrad^2 mm^2), where x stands for photons/s, J/s, or J. In the graphs where a comparison with a flat single-crystal spectrometer (SC) is presented, similar characteristics of the SC were computed using a previously published code.[7]

Unless stated otherwise, the properties of the spectrometers were calculated for diffracting crystals ADP (101), single spectral line Al $Ly\alpha_{1/2}$ with a symmetric Lorentzian profile and the relative width $\Delta\lambda/\lambda=1\times10^{-3}$, source size 100×100 μm^2, source-to-detector distance $L=100$ mm, and vertical divergence angle $\varphi=5°$ (which corresponds to $\theta_0=42.6124°$).

As a starting point for the majority of applications, the linear dispersion of the DCV given by $D_{\text{lin}}=-L/(\lambda\cos\varphi\sin\varphi)$ is shown in Fig. 4. Up to approximately $\varphi=6°$, the linear dispersion of the DCV at $L=100$ mm is even higher than that calculated for the SC at $L=1000$ mm (for $L=100$ mm, the linear dispersion of the SC is only 12.7 mm/Å). Hence it is obvious why the source size does not limit the spectral resolution of the DCV so strongly at relatively small values of L.

The dependence of the spectral resolution on φ (for convenience it is also calculated as a function of the wavelength difference $\lambda-\lambda_0$) is shown for several source sizes in Fig. 5. In accordance with the variable dispersion, the resolution decreases with φ and also its degradation at large source

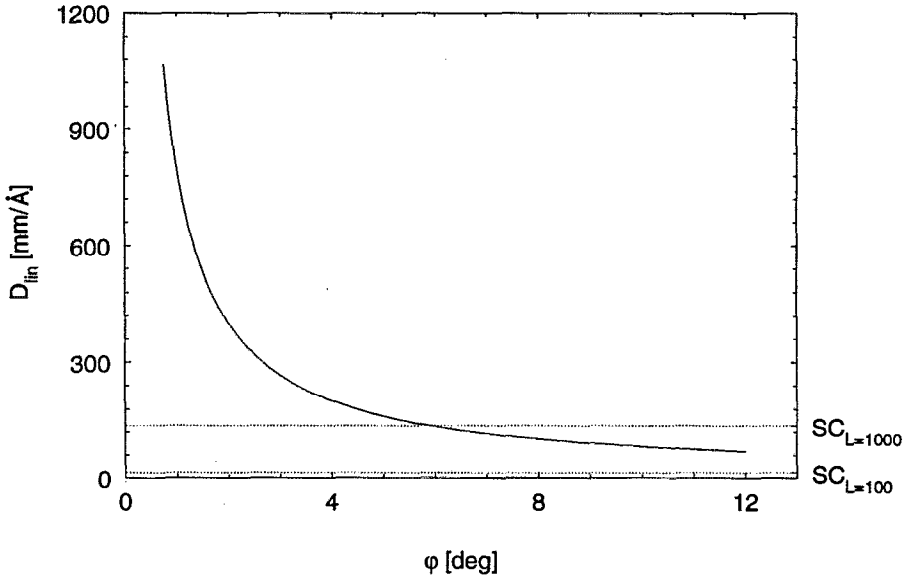

FIG. 4. The linear dispersion of the DCV as a function of angle φ. For comparison, the linear dispersion of the flat single-crystal spectrometer is shown at the source-to-detector distances 100 and 1000 mm.

sizes is evident. The most important fact is that the resolving power of the DCV may exceed the ultimate value $R=8200$ given by the FWHM of the SCDP (6.4 mdeg). (The angular width of the SCDP 4.5 mdeg stated in our previous papers[10,16] was 30% smaller; the new value was recalculated using an updated set of crystallographic data.[15]) As discussed in Sec. III, this corresponds to the narrowing of the composite rocking curve (4.9 mdeg) due to the twofold reflection on the crystals. At smaller source sizes and angles φ, the resolution approaches the value $R=10\,600$ given by this CRC diffraction limit.

For the standard parameters given above the spectral resolution exceeds the SCDP limit in the range of 27.4 mÅ about the central wavelength. This range is fully adequate to record spectral line profiles with relative widths up to approximately 2×10^{-3}. The wings of the broader profiles

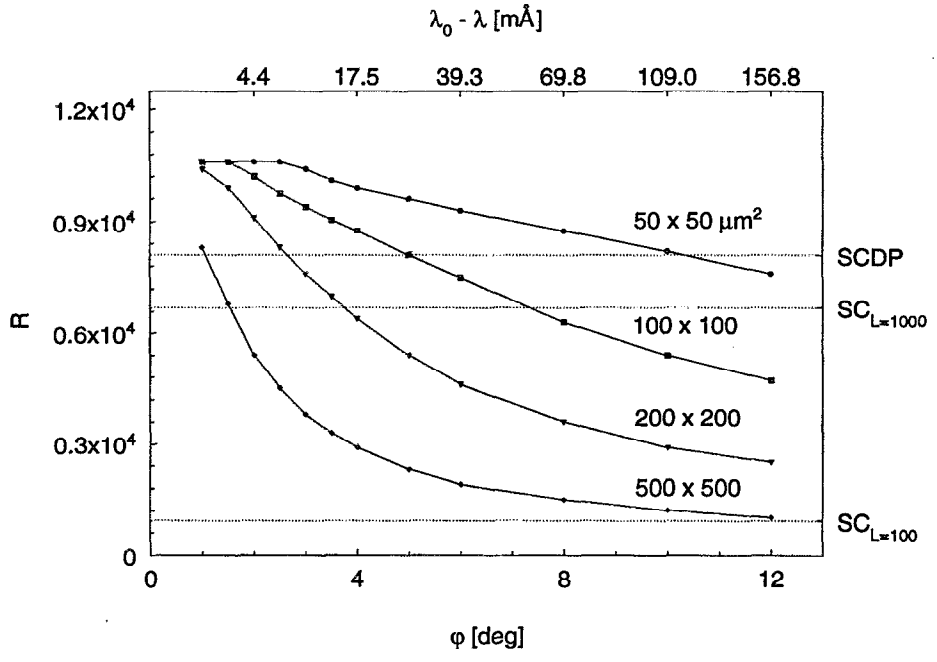

FIG. 5. Spectral resolution of the DCV plotted for several source sizes as a function of the angle φ or as a change of the wavelength related to that of the central ray. Also shown is the single-crystal diffraction limit (corresponding to $R=8200$) and the resolution of the SC for the source size 100×100 μm^2 at distances $L=1000$ ($R=6700$) and 100 mm ($R=910$).

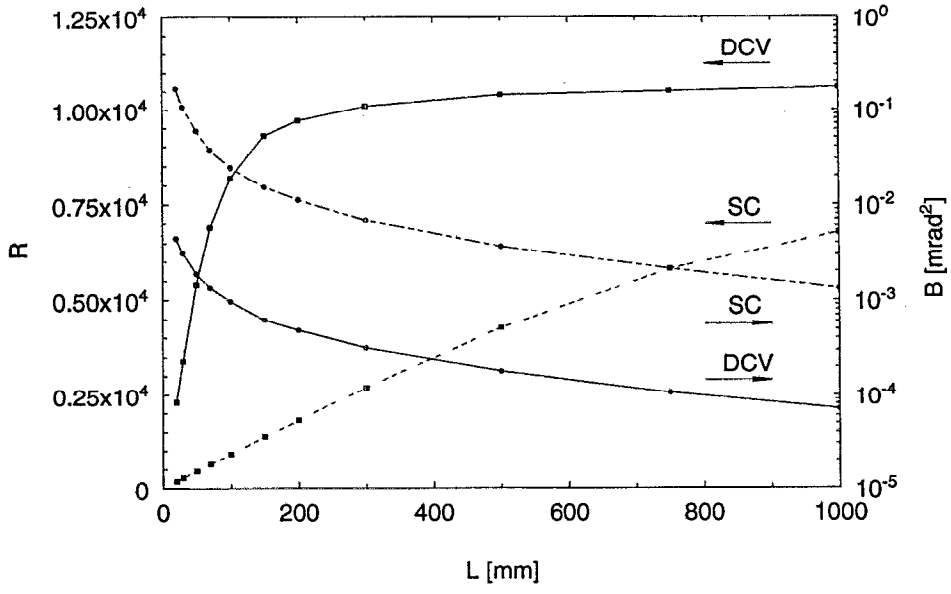

FIG. 6. Spectral resolution R and luminosity B of the DCV (solid line) and SC (dashed) as a function of the source-to-detector distance L.

would be measured with a slightly lower resolution but this would still exceed that of the SC even at large distances L.

This may be seen from Fig. 6, where the spectral resolution and luminosity of the DCV and SC are plotted as a function of distance L. The resolution of the DCV grows rapidly at first and then slowly approaches its limiting value. Due to the practically linear decrease of the luminosity with L, the source-to-detector distance should not exceed the value $L \cong 150$ mm. In contrast, the spectral resolution of the SC increases in the range of L shown; however, its value at $L = 1000$ mm is still well below the SCDP limit. The ratio of luminosities of the SC and DCV at a given distance L drops from 38 at $L = 20$ mm to 19 at $L = 1000$ mm, so the collecting efficiency of the SC is much higher. If the given value of the spectral resolution is required to detect the fine spectral features, the corresponding luminosities of both schemes can be determined from Fig. 6. Generally speaking, at a modest level of spectral resolution the SC provides higher intensities; at $R \cong 6000$ the luminosities of the DCV and SC are equal; for still finer resolution the DCV provides higher collection efficiency. The situation also changes dramatically if spectroscopic data are required with 1D spatial resolution. To achieve a spatial resolution of 10 μm, the SC must include a horizontal slit of corresponding width. The luminosities of both instruments calculated for the standard parameters are then practically the same but the DCV provides almost one order of magnitude higher spectral resolution. Obviously the full set of the characteristics must be taken into account to optimize the experimental layout.

The influence of the horizontal source size on the normalized intensity distribution at the detector is shown in Fig. 7. Since this distribution is symmetrical about the axis z', the intensity is therefore plotted as a function of positive y' only. In this figure the horizontal source width W varies from 1 to 100 μm for a constant vertical source size 10 μm. The intensity distribution computed for $W = 1$ μm is comparable with the point spread function discussed before; it broadens with increasing W and starting from $W \cong 30$ μm a distinct plateau appears around the signal maximum. The actual values of intensity maxima I_{max} are shown in Fig. 8. As expected, the I_{max} increases with W, and saturation occurs again at $W \cong 30$ μm. The maximum intensity also grows proportionally to the source size in the vertical direction; up to source size 500 μm (which covers most cases of practical importance), this dependence is linear to within 6% and is therefore not plotted here.

V. TRANSFER OF SPECTRAL LINES

Individual elements of a spectrographic system are characterized by their transmission functions. The produt of these functions gives the line transmission function of the instrument,[5] defined as the ratio of the integrated diffracted intensity at the detector to the source radiance i_0 with the

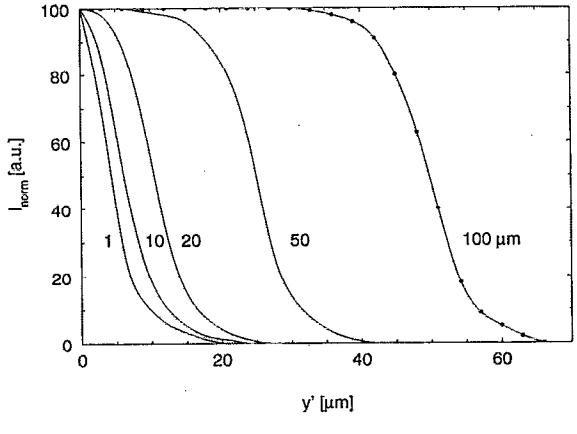

FIG. 7. Normalized intensity distribution I_{norm} at the detector plane plotted for different horizontal source sizes.

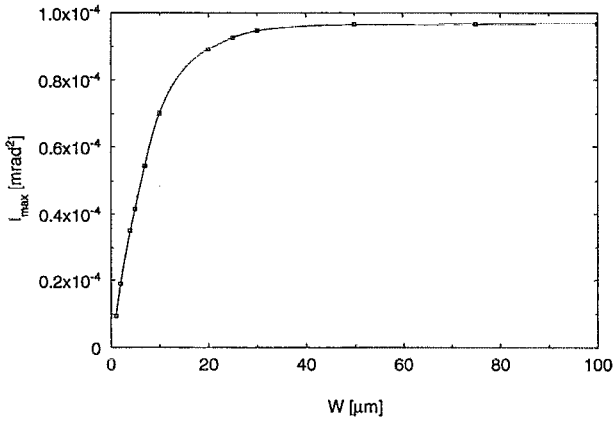

FIG. 8. Intensity maximum at the detector I_{max} vs the horizontal source size W. The vertical source size remains constant (10 μm).

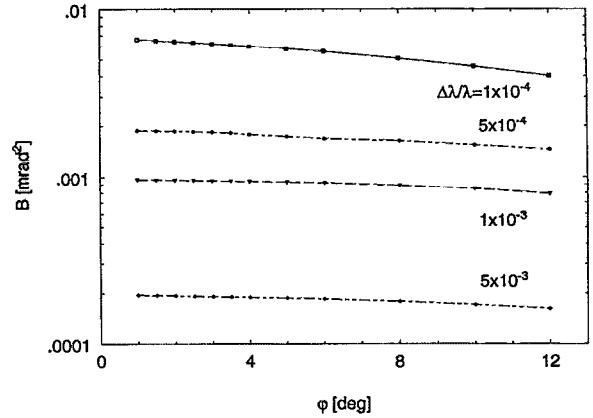

FIG. 10. The DCV luminosity B plotted as a function of the angle φ for λ=7.1749 Å and several relative spectral linewidths $\Delta\lambda/\lambda$.

assumption that it emits an isolated spectral line. From Eq. (6), the line transmission function T_l of the DCV may be written as

$$T_l = \int_{y'} \int_{z'} P(y',z')/i_0 \, dy' \, dz'. \tag{10}$$

For the standard calculation parameters, the dependence of T_l on the angle φ is shown in Fig. 9. The nonlinear character of T_1 follows from the properties of the CRC discussed in Sec. III. The value of T_l decreases at small angles φ because close to the detector axis a part of the profile is not detected on the long-wavelength side as a consequence of Eq. (3).

In spite of this nonlinearity, the reconstruction of the detected spectra is relatively simple and provides good results. The intensity distribution in the plane (y',z') can be easily recalculated for the wavelength scale by means of Eq. (3) if λ_0 and L are known; in the design of an experiment, care must be taken to determine these parameters with sufficient precision.

A finite detector pixel size (given by the real pixel size of the CCD camera or by a system of microdensitometer slits when using x-ray film) is an additional factor which may influence the smearing of spectroscopic data. Its horizontal dimension $\Delta y'$ limits the spatial resolution; the vertical dimension $\Delta z'$ determines the width of the spectral window. This follows from the fact that the signal P_d detected in a given pixel may be expressed as

$$P_d = \int_{\Delta y'} \int_{\Delta z'} P(y',z') dy' \, dz'. \tag{11}$$

With increasing φ, the dispersion decreases so the wavelength interval corresponding to the given pixel size increases. Consequently, the spectral smearing also slightly increases but it still does not distort the spectral profile significantly.

The other factors determining the spectral distortion are the source size, the shape of the CRC, and the relative width of the spectral line. The influence of different combinations of these parameters on the resulting apparatus distortion were again determined from the ray tracing procedure.

Probably the most important characteristic of the DCV to emerge from these computations is that the luminosity (i.e., the intensity corresponding to the maximum of the spectral line) depends relatively slowly on the angle φ. As may be seen in Fig. 10, for $\Delta\lambda/\lambda = 1\times10^{-3}$ the decrease in intensity from φ=1° to φ=10° is about 12%, which is mostly due to the partial crossing of polarization vectors (10%). In contrast, at $\Delta\lambda/\lambda = 1\times10^{-4}$ the intensity drops by approximately 25%, i.e., at higher angles φ this effect should be taken into account.

The measured spectrum is a convolution of the true spectrum and the apparatus smearing function. To estimate the instrumental distortion, we have performed a computer-simulated experiment for different shapes and relative widths of the spectral line profiles. An example of such calculation is presented in Fig. 11. A theoretical profile of the Al $Ly\alpha_{1/2}$ emission (solid line) was approximated by a Lorentzian function with the relative width at FWHM $\Delta\lambda/\lambda = 7.9\times10^{-4}$ and an asymmetry a=0.6. These parameters correspond to the postprocessed hydrodynamics simulation[17] of x rays emitted from a LPP generated by a single laser beam (80 J, 0.53 μm, 1.2 ns) normally incident on a thick Al foil at flux density 3×10^{14} W/cm^2. X rays were observed at 60° to the target normal so that the line shape was modified

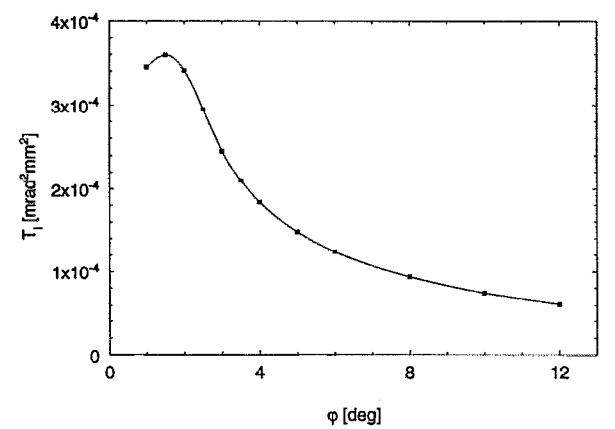

FIG. 9. Line transmission function T_l of the DCV vs the angle of vertical divergence φ.

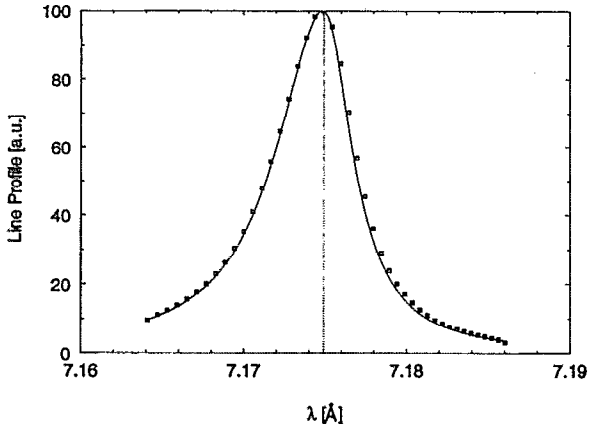

FIG. 11. Computer-simulated experiment—a comparison of the spectral line profile detected by the DCV (points) with the theoretical one (solid line).

considerably by the Doppler broadening and subsequent transport through the plasma.[18] The transmission of this radiation through the DCV was simulated for $L=100$ mm and ADP (101) crystals set at 85.25°, corresponding to $\varphi=5.15°$. The signal distribution at the detector was converted to the wavelength scale using the method described above. The resulting spectral profile is shown in Fig. 11 by points where both curves are normalized to a peak value of 100. The wavelength shift of the profile peak is smaller than the precision of the calculation (the spectral resolution for the parameters specified above is 6400); the observed spectral line is 5% wider and is more asymmetric with $a=0.63$. The spectral profile does not require deconvolution since the instrumental distortion is negligible.

This, however, need not always be true. For a symmetrical line at the same wavelength but with a much narrower relative width $\Delta\lambda/\lambda=1\times10^{-4}$, we have found that the relative shift of the line center is at a still acceptable level of 2×10^{-5}, but its width $\Delta\lambda$ has more than doubled (by 107%). In this case, the spectral resolution of the instrument is too low. The situation might slightly improve at smaller angles φ where the spectral resolution increases (see Fig. 5), but generally to get high-precision data for such narrow lines, crystals with even higher resolving powers are necessary.

VI. INSTRUMENT PERFORMANCE, VERIFICATION OF COMPUTED CHARACTERISTICS

The first-generation DCV designed at the Prague Institute of Physics was used in laser-plasma experiments at the Central Laser Facility of the Rutherford Appleton Laboratory. The description of the instrument, examples of the spectra recorded, and their interpretation are given elsewhere,[11,12,18] and so are not repeated here. In the following paragraphs, the precision attainable for wavelength measurement is discussed and selected results of the DCV tests are shown.

The precision of the wavelength determination $\Delta\lambda_m$ may be estimated by differentiating Eq. (3). Using the Bragg condition, we obtain

$$\Delta\lambda_m/\lambda=\Delta d/d+\Delta\theta_0/\tan\theta_0+\tan\varphi\Delta\varphi, \tag{12}$$

where Δd, $\Delta\theta_o$, and $\Delta\varphi$ are uncertainties in the given parameters. $\Delta\lambda_m$ obviously depends on several factors which can be divided into two groups: the first is connected to the characterization of the crystals used (determination of interplanar spacing d, tilt of the diffraction planes to the crystal surface); the second is connected with the alignment of the instrument (precision of the mutual angular setting of the crystals and the detector, determination of the source-to-detector distance) and data processing (readout of corresponding coordinates at the detector).

The interplanar spacing of the crystals used is routinely measured with a relative precision of 10^{-4}–10^{-5} (exceptionally[19] even 10^{-7}) and corrected for refractive index decrement by well-known formulas and optical data.[20] The angular misalignment between the diffraction planes and the polished surface of commercially available crystals is usually about 1 arcmin or less. If it is higher, it must be taken into account in the optical adjustment of the crystals; the angle between the diffraction planes of both crystals may be set to an accuracy of 20–60 arcsec by using a precision rotation stage and autocollimator. The source-to-detector distance via the crystals can be determined with a precision of 0.2–0.4 mm. This may be achieved by a proper design of the instrument with predetermined positions of the source and the detector or, alternatively, by the measurement of the spectra at two distances L and $L+\Delta L$, where ΔL is known and long enough; the value of L can then be calculated by comparing the spacing of the corresponding spectral features. The precision of the z'-coordinate readout depends on the pixel definition at the detector. If x-ray film is used, this precision is given by the microdensitometer scan and may be estimated as 5 μm. The tilt of the diffraction planes and of the detector from an ideal vertical position may also contribute to $\Delta\lambda_m$ but this is still negligible even for a tilt as large as 1°.

The DCV can be used both for absolute and relative measurements of wavelengths. For absolute measurements, the wavelengths of the spectral lines or absorption edges are determined from the full set of geometric parameters known within the limits above. The overall precision may be estimated as $\Delta\lambda_m/\lambda=(1-5)\times10^{-4}$, the main contribution of this being introduced by Δd and $\Delta\theta_0$. For relative measurements, the spectral features investigated are related to the reference wavelength; this mode of measurement is commonly used, e.g., for the determination of relative positions, shifts, and widths of spectral lines. If both the reference feature and that under study are within the spectral range of the instrument (set by maximum value of φ which is limited either by the intensity drop discussed in Sec. III or by the dimensions of the crystals or the detector), then according to Eq. (3) their relative position on the wavelength scale can be determined without knowing either d or θ_0. The sensitivity of such measurements of the spectral line positions and shifts may be estimated as $\Delta\lambda_m/\lambda=1\times10^{-5}$; note that the accuracy of the determination of the spectral linewidths is limited by the CRC of the instrument.

The spectral resolution of the DCV was demonstrated in

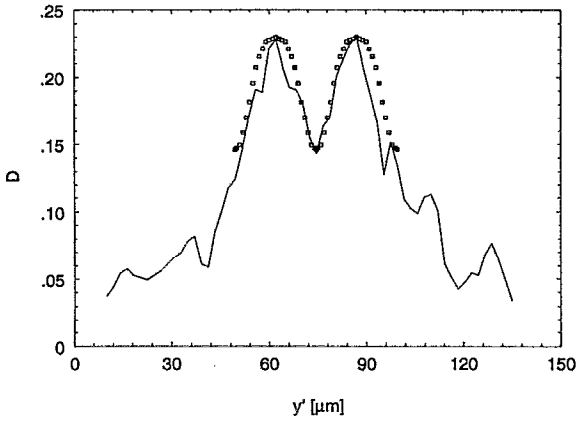

FIG. 12. Modulation of the film density D in the direction y' perpendicular to the spectral dispersion which was introduced by a fine grid positioned 1 mm from the source. The fit of experimental (solid curve) and theoretical data (points) confirms the spatial resolution of the DCV.

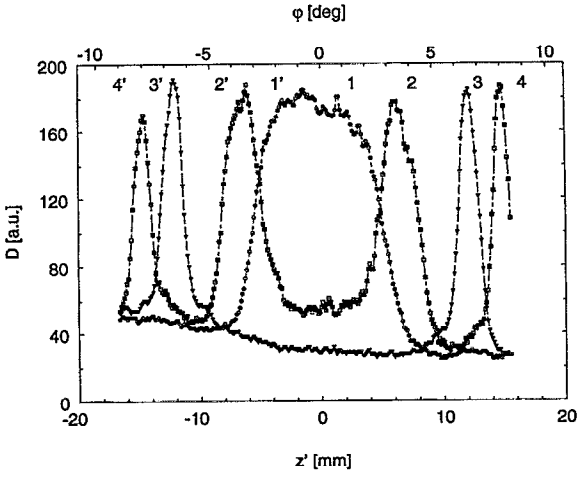

FIG. 13. Microdensitometer lineouts of the spectral line $1s^2S-2p^2P$ of hydrogenlike aluminium taken at the angles of vertical divergence φ=0.8°, 3.3°, 6.6°, and 8° (lines 11′, 22′, 33′, and 44′, respectively).

the previous experiments.[11,18] Only a lower limit of about 3000 could be estimated for resolution obtainable experimentally since well-defined narrower spectral features were absent. For the parameters shown in Fig. 5, i.e., focal spot diameter on the target 200 μm, vertical divergence angle 5°, and source-to-detector distance 100 mm, the theoretical value approaches 5400.

The spatial resolution in the direction perpendicular to the dispersion plane was verified by observing the spectra with a fine grid inserted between the source and the first crystal. The experiment was performed on the VULCAN neodymium glass laser at RAL, using a single beam providing a 1.2 ns (FWHM) pulse with 80 J at 0.53 μm. The radiation was focused onto a 10 μm thick aluminum foil with irradiance 3×10^{14} W/cm^2. The Al $Ly\alpha$ doublet ($1s^2S-2p^2P$) was detected in a single shot using two ADP (101) crystals and x-ray film (Kodak Industrex-AX). The total target-to-film distance was 120 mm, the grid with a period of 25 μm, and a bar thickness 6 μm was set at a distance of 1 mm from the focal spot.

In plasmas generated by laser pulses as above, the Doppler motion smears the Al $Ly\alpha$ doublet into a single line, the profile of which is further modified by the transport of radiation through the plasma.[18] The distribution of the optical density on the film in the direction perpendicular to the spectral dispersion is shown in Fig. 12. The lineout was taken close to the maximum of the spectral line profile. In the range shown the optical density is linearly proportional to the intensity; therefore these experimental results (solid line) could be directly compared with the modulation of the signal distribution predicted from the theory of the instrument (points). The coincidence between the curves is very close; the drop between the maxima agrees within 2% with the results of ray tracing calculation. The same intensity distribution would be observed by assuming that the FWHM width of the point spread function is 10.2 μm, which corresponds fully to that expected from the product of the horizontal width of the composite rocking curve and the given source-to-detector distance.

This experiment confirmed two important facts: First, the DCV provides the spatial resolution in accordance with theory outlined in Sec. III. Second, the simplifying assumptions of the ray tracing procedure, which neglect the finite penetration of the radiation under the surface of flat crystals (and consequently the broadening of the diffracted beam), do not substantially influence the precision of the computed characteristics. As mentioned above, we could not test the ultimate spectral resolution directly. However, the spectral and spatial resolution are so intricately linked that since the spatial resolution is as predicted (i.e., the crystals are acting dynamically), we have increased confidence that the spectral resolution calculations are correct.

The last figure presented shows a microdensitometer lineout of the $Ly\alpha$ doublet of aluminium recorded at different angles θ_0 corresponding to the angles of vertical divergence φ=0.8°, 3.3°, 6.6°, and 8°. The spectra were taken under the same experimental conditions as above except that the target-to-film distance was 105 mm. The x-ray film was moved transversely between the individual shots by approximately 2 mm except that spectral lines 2 and 4 were inadvertently recorded on the same track.

In Fig. 13, the character of the registered spectra is clearly seen. Two sets of spectral lines are recorded symmetrically about the central wavelength with the dispersion strongly depending on the vertical divergence. For the lowest angle φ, the double spectrum merges in one broad line. The apparent spectral linewidth on the film decreases with φ but after recalculation to the wavelength scale, the true widths (FWHM) of curves 2, 3, and 4 remain constant within 3.5% (standard deviation). Figure 13 also demonstrates the quasi-constant luminosity of the DCV; the observed differences in the maxima of the spectral lines may be attributed to the limited reproducibility of the individual laser shots, to nonhomogeneous reflectivity along the crystal surface, and possibly also to the anisotropic character of the plasma emission.

This investigation has confirmed the main computed

characteristics of the vertical dispersion variant of the double-crystal spectrometer. Two flat crystals, which are used in the DCV as the dispersive elements, can be prepared with a high degree of perfection; this is why we have not found any substantial differences between the observed and theoretical instrumental parameters.

VII. DISCUSSION

The unique properties make the vertical dispersion variant of the double-crystal spectrometer suitable for detailed investigation of x-ray emission from laser-produced plasmas. The use of two crystals provides extremely high dispersion, the high spectral resolution exceeding the limit set by the single-crystal diffraction pattern and one-dimensional imaging of the plasma source.

Two sets of identical spectra are recorded symmetrically disposed about the central wavelength and this provides a unique possibility to accurately measure the spectral line positions and shifts. The precision of relative and absolute wavelength measurement may easily reach 1×10^{-5} and $(1-5)\times10^{-4}$ λ, respectively. In most of the cases encountered, the distortion of the measured spectra is negligible and the spectral line profiles need not be deconvoluted. By using a calibrated detector and well-characterized crystals with the reflective properties described by the dynamic theory of x-ray diffraction, the DCV records the intensity distribution of spectral lines on an absolute scale related to the source radiance; this is extremely important when studying, e.g., radiative transport in plasmas.[18]

Routine x-ray diagnostics of LPPs are frequently carried out by instruments with moderate parameters. The application of the DCV which is easy to build (using good commercially available crystals and standard rotation stages) and easy to align may improve the situation considerably. The analysis described above provides a comprehensive theoretical basis for using the DCV in high-precision spectroscopy of laser-produced plasmas.

ACKNOWLEDGMENTS

This program is supported by Grant Agencies of the Czech Republic and of the Academy of Sciences under Grants No. 202/93/1023 and No. 110427. The substantial part of this work has been performed during the stay of one of the authors (O. R.) in Jena with the COST Go West Scheme under Contract No. ERB-CIPA-CT-93-0632. For the experimental part of this work, two of the authors (O. R. and E. F.) were partially supported by the visiting fellowship from the UK Science and Engineering Research Council under Grant No. GR/H02059. The authors gratefully acknowledge the assistance of T. Missalla, D. Neely, and the staff of the Central Laser Facility of the Rutherford Appleton Laboratory in performing the experiments, and fruitful discussions with R. J. Hutcheon and S. J. Rose.

[1] A number of authors have reviewed this subject. The reader is referred to the survey articles by M. H. Key and R. J. Hutcheon, Adv. At. Mol. Phys. **16**, 201, (1980); V. A. Boiko, A. V. Vinogradov, S. A. Pikuz, I. Yu. Skobolev, and A. Ya. Faenov, J. Sov. Laser Res. **6**, 85 (1985); A. Hauer, N. D. Delameter, and Z. M. Koenig, Laser Particle Beams **9**, 3 (1991), and references therein.
[2] R. Marjoribanks, M. C. Richardson, P. A. Jaanimagi, and R. Epstein, Phys. Rev. A **46**, 1747 (1992).
[3] A. Hauer, J. D. Kilkenny, and O. L. Landen, Rev. Sci. Instrum. **56**, 803 (1984).
[4] E. Förster, K. Gäbel, and I. Uschmann, Rev. Sci. Instrum. **63**, 5012 (1992).
[5] B. L. Henke, H. T. Yamada, and T. J. Tanaka, Rev. Sci. Instrum. **54**, 1311 (1983).
[6] B. S. Fraenkel, Appl. Phys. Lett. **41**, 234 (1982).
[7] O. Renner and M. Kopecký, Czech. J. Phys. **40**, 1107 (1990).
[8] O. Renner, M. Kopecký, E. Krouský, E. Förster, and J. S. Wark, Proc. SPIE **1980**, 87 (1993).
[9] J. Hrdý, Czech. J. Phys. B **18**, 532 (1968).
[10] O. Renner, Proceedings of the Conference on X-ray Inner Shell Processes, Leipzig, 1984, Book of Abstracts (unpublished), p. 366.
[11] H. He, J. S. Wark, E. Förster, I. Uschmann, O. Renner, M. Kopecký, and W. Blyth, Rev. Sci. Instrum. **64**, 26 (1993).
[12] J. S. Wark, H. He, O. Renner, M. Kopecký, E. Förster, and T. Missalla, J. Quant. Spectrosc. Radiat. Transfer **51**, 397 (1994).
[13] O. Renner and M. Kopecký, Laser Particle Beams **10**, 841 (1992).
[14] A. H. Compton and S. K. Allison, *X-Rays in Theory and Experiment* (Van Nostrand, New York, 1935).
[15] G. Hölzer (private communication).
[16] J. Hrdý, Czech. J. Phys. B **35**, 401 (1985).
[17] S. J. Rose (private communication).
[18] J. S. Wark, A. Djaoui, S. J. Rose, H. He, O. Renner, T. Missalla, and E. Förster, Phys. Rev. Lett. **72**, 1826 (1994).
[19] J. Härtwig, S. Grosswig, P. Becker, and D. Windisch, Phys. Status Solidi A **125**, 79 (1991).
[20] B. L. Henke, E. M. Gullikson, and J. C. Davis, At. Data Nucl. Data Tables **54**, 181 (1993)